

# **Topography, jets, and eddy mixing in the Southern Ocean**

Jianhua Lu<sup>1</sup> and Kevin Speer<sup>1,2</sup>

<sup>1</sup> Geophysical Fluid Dynamics Institute, the Florida State University, Tallahassee, Florida, U.S.A

<sup>2</sup> Department of Earth, Ocean, and Atmospheric Science, Florida State University, Tallahassee, Florida, U.S.A

(Submitted to J. Mar. Res. , Dec. 3<sup>rd</sup>, 2009)

Corresponding Authors Address: Jianhua Lu, Geophysical Dynamical Fluid Institute, Florida State University, 018 Keen Building, Tallahassee, FL 32306.

Email: [lu@gfdi.fsu.edu](mailto:lu@gfdi.fsu.edu)

Kevin Speer, Department of Earth, Ocean, and Atmospheric Science, Florida State University, Tallahassee, FL 32306

Email: [kspeer@ocean.fsu.edu](mailto:kspeer@ocean.fsu.edu)

## ABSTRACT

The relation between topography, jets, and the 3D structure of patchy eddy-induced mixing in the Southern Ocean is analyzed descriptively by applying diagnostic methods to output from the Southern Ocean State Estimate. A localized cumulative probability density function method is developed to verify the use of Nakamura (2001)'s mixing efficiency in the ocean. Both methods reveal enhanced eddy mixing at mid-depths. The spatial pattern of the mid-depth enhancement of eddy mixing is primarily linked to the merging of multiple jets embedded in the Antarctic Circumpolar Current over topography. We suggest that enhanced eddy mixing over topography is due to locally enhanced baroclinicity and instability within the wake, itself partly due to the convergence of eddies in merging branches of the ACC. Interaction of barotropic and baroclinic eddies may be important to setting the strength and vertical structure of eddy mixing associated with topography.

# 1. Introduction

Mesoscale eddy fluxes are thought to have a significant role in setting the strength of the Antarctic Circumpolar Current (ACC) and the meridional overturning and subduction, hence carbon, nutrient, and other tracer fluxes. Estimating and simulating their effects in coarse resolution climate models is key to producing accurate forecasts of climate. There are continuing debates on the eddy diffusivity in the Southern Ocean, about not only its intensity but also its spatial structure. Different descriptions of eddy fluxes in terms of diffusivities have been found; these differences influence the behavior of eddies in models and reveal shortcomings in the explanation of the underlying physical mechanisms responsible for eddy-induced ocean mixing.

One approach for estimating eddy diffusivity is based on the Lagrangian eddy statistics such as the turbulent dispersion (see reviews by Garrett, 2006; LaCasce, 2008). Sallee *et al.* (2008) estimated the eddy diffusivity in the Southern Ocean by a Lagrangian analysis of surface drifter observations and proposed that surface eddy diffusivity is related to eddy kinetic energy (EKE) in energetic regimes, but otherwise is relatively constant outside those regimes over most of the Southern Ocean.

Another method is the effective eddy diffusivity method (Nakamura, 1996) in which, by introducing an area coordinate, and based on the area-preserving nature of advection, the advection-diffusion equation is reduced to a pure diffusion equation. By the use of equivalent length, the effective diffusivity method diagnoses the irreversible mixing generated by the eddy stirring which stretches and folds the tracer contours. Marshall *et al.* (2006) estimated the effective eddy diffusivity in the Southern Ocean, and

they found that the eddy diffusivity is suppressed at the core of jets while enhanced on the equatorial flank of the Antarctic Circumpolar Current. Abernathey *et al.* (2010) further applied the Nakamura method to estimate the effective diffusivity in three dimensions in the Southern Ocean, and argued that the effective diffusivity is enhanced in the vicinity of the steering level of baroclinic waves, which is shallow on the equatorial flank of the ACC and deeper along the ACC axis.

Note that different methods give rise to different estimates of the eddy diffusivity in the Southern Ocean. The estimate of Sallee *et al.* (2008), for example, is larger in the ACC than the effective diffusivity of Marshall *et al.* (2006). Sallee *et al.* (2008) discuss at length the possible causes of the differences, such as different averaging methods and mapping strategies.

The comparison of different methods also suggests different spatial structures of the eddy diffusivity. For instance, Sallee *et al.* (2008) found mixing to be approximately constant over most of the ACC, but significantly linked to EKE where EKE is large, typically in western boundary currents extending into the Southern Ocean. Marshall *et al.* (2006) showed strong surface effective eddy diffusivity on the equatorial flank of the ACC jets; however, with their zonally integrated measure they were unable to map the spatial distribution but estimated the cross-stream, general north-south variation. Griesel *et al.* (2010) argue that EKE alone does not adequately describe mixing structure, particularly with respect to depth dependence, and they find no deep enhancement.

The difference in the spatial structure in the eddy diffusivity leads to different explanations for the role of jets in eddy diffusivity. The analysis of satellite altimetric

data combined with scaling theories of geostrophic eddies tends to suggest that jets may enhance the eddy diffusivity through the associated eddy activity and EKE (e.g., Stammer, 1998). Marshall *et al.* (2006) and Abernathey *et al.* (2010) promote the view that jets, with their maximum speed exceeding eddy phase speed, tend to suppress mixing. Recently Ferrari and Nikurashin (2010) developed a quasi-geostrophic mixing length theory of eddy-induced mixing. In the theory, the mixing length (and the eddy diffusivity) is proportional to  $\sqrt{EKE}$ , but the presence of a mean flow (or a broad jet) acts to reduce the mixing length hence eddy diffusivity. Naveira-Garabato *et al.* (2009) further argue that any suppression of mixing may break down in narrow, non-parallel mean jets.

While the methods mentioned above explicitly estimate the eddy diffusivity, there are also some other approaches that aim to analyze the mixing structure of the ocean, though not explicitly giving the estimate of eddy diffusivity, by using a dynamical-system-theory based Lagrangian description of transport and mixing. Among them are the Finite Time Lyapunov Exponents (FTLE) method (Waugh and Abraham, 2008) and the Finite Size Lyapunov Exponents (FSLE) method (d’Ovidio *et al.*, 2004). Waugh and Abraham (2008) calculated the surface FTLE over the global ocean and found it to be related to the distribution of EKE.

The differences in estimates of both the intensity and spatial structure of the eddy-induced stirring and mixing raise some interesting questions regarding the role of the ACC in eddy diffusivity: is it better to think of the ACC as a region of generally elevated mixing, as suggested by some Lagrangian dispersion statistics, or of generally suppressed mixing as suggested by Marshall *et al.* (2006) and Ferrari and Nikurashin (2010)? What is the physical meaning of the contrary views on the mixing, or are they only artifacts of

the methods? How can one describe the localized distribution of irreversible mixing in the ocean?

It is known that oceanic fronts are regions of strong EKE, but the mixing rate must vary strongly in different flow regimes such as bands of weak flows, reversals and strong fronts. While the sharp PV/tracer gradient associated with the fronts and observed near jet cores suggests the jets are barriers to mixing (Bower and Lozier, 1994), the mixing has long been believed to occur near the critical surface associated with a baroclinic unstable jet (Bower, 1991; Lozier and Bercovici, 1992; Pratt *et al.*, 1995; Lozier *et al.*, 1997; Boss and Thompson, 1999). By averaging or mapping along fronts, the stream-wise averaged eddy diffusivity has an important property in that it retains the difference in diffusivity or mixing between the jet core and the critical surface (Nakamura, 1996). Unlike in the atmosphere where the scale of unstable baroclinic eddies is  $O(1000 \text{ km})$ , the mesoscale eddies and associated jets in the ocean are on much smaller scales. The eddy-induced mixing may be much more localized, for example, in western boundary currents and their extensions, gyre boundaries (e.g. Wiggins, 2005) or by interior topography (Macready and Rhines, 2001). Therefore a tracer (such as PV) contour on which the area-average is made for Nakamura's effective diffusivity may span different dynamic regimes. Localized splitting and merging of the ACC jets may also be important for generating along-stream structure in mixing (Thompson, 2009). Therefore the effective diffusivity method may combine different dynamic regimes into one single estimate (as remarked by Sallee *et al.*, 2008), and blurs the local signal of eddy mixing. Schuckburgh *et al.* (2009) developed a more localized effective diffusivity calculation on small patches of the ocean by modifying the velocity field to create a re-entrant zonal-

periodic channel with no flow out of the meridional boundaries. In their calculation for the Pacific sector of the Southern Ocean, Schuckburgh *et al.* (2009) found both the suppression of eddy diffusivity by strong mean flow and larger mixing values that may be locally enhanced over areas with stronger bottom topography in the ACC region.

In this paper we seek to demonstrate that the ACC is a complex system of barriers and well-mixed zones and bands, and that the lateral mixing is enhanced where the ACC jets interact with topography (Figure 1). In doing so, we introduce two methods that could be used to account for the localized nature of ocean mixing and compare them with the FSLE and relative dispersion methods.

The outline of our paper is as follows. In section 2 we introduce the methodology and data, followed in section 3 by the comparison of the diffusion or mixing in the Southern Ocean described by these methods and possible causes for the difference. In section 4, we analyze the horizontal and vertical structure of eddy mixing in the ACC. The role of topography in enhancing the isopycnal mixing will be presented in Section 5. Conclusions and discussion are provided in Section 6.

## 2. Methodology and data

### a. The Mixing efficiency ( $M_e$ ) index

Nakamura (2001) proposed a new framework to address the local and inhomogeneous nature of eddy-induced irreversible mixing by partitioning the eddy flux into components normal and parallel to the local tracer gradient. Here we briefly introduce the method; for a more detailed derivation and discussion refer to Nakamura

(2001). After averaging, a modified Eulerian-mean equation for the advection-diffusion of tracer concentration  $q$  is obtained:

$$\frac{\partial \bar{q}}{\partial t} + \nabla \cdot (\bar{\mathbf{v}}^* \bar{q}) = \nabla \cdot (K^* \nabla \bar{q}) \quad (1)$$

where the bar denotes an Eulerian average,  $\bar{\mathbf{v}}^*$  is a nondivergent effective transport velocity, with

$$\bar{\mathbf{v}}^* = \bar{\mathbf{v}} + \bar{\mathbf{v}}_e, \quad \nabla \cdot (\bar{\mathbf{v}}^*) = 0.$$

where  $\bar{\mathbf{v}}_e$  is the additional transport velocity associated with the antisymmetric part of diffusivity tensor. The diffusivity  $K^*$  is further partitioned in another form by introducing the tracer variance equation:

$$K^* \equiv K_k + K_m, \quad (2a)$$

$$K_k = \frac{\frac{\partial}{\partial t} \overline{|q|^2} + \nabla \cdot (\overline{\mathbf{v} q^2} - D_m \nabla \overline{|q|^2})}{2 |\nabla \bar{q}|^2}, \quad (2b)$$

$$K_m = \frac{D_m |\nabla \bar{q}|^2}{|\nabla \bar{q}|^2} = D_m M_e. \quad (2c)$$

where  $D_m$  is the molecular diffusivity, Nakamura (2001) pointed out that the term  $K_k$ , which could take either sign, is related to the dispersion of tracer surfaces due to eddy advection.  $K_m$  is positive by construction. It arises from molecular diffusion, but is amplified by the factor  $M_e$ .  $M_e$  is called the “mixing efficiency” (Nakamura, 2001), representing the eddy enhancement of irreversible diffusion, and is analogous to similar

amplifying factors in models of vertical mixing. Nakamura (2001) diagnosed the mixing efficiency in the stratosphere and found suppressed mixing and localized barriers along the jet axes at the midlatitude tropopause. Here we apply the method to a Southern Ocean reanalysis (SOSE, see below) with the aim to diagnose the structure of mixing due to mesoscale eddies in the ocean.

### *b. The Localized Cumulative Probability Density Function (CDF) method*

Because the area (mass) enclosed by tracer concentration  $q_* \leq q$ , normalized by the total area (mass), is the cumulative density function (CDF) of  $q$  (Nakamura, 2008), the equation for the change of area

$$A(q,t) \equiv \int_{q^* \leq q} dS \quad (3)$$

in the effective diffusivity formalism of Nakamura (1996) is equally applicable to the

$$\text{CDF } C(q,t), \text{ with } C(q,t) \equiv \frac{1}{A_0} \int_{q^* \leq q} dS$$

i.e.

$$\frac{\partial}{\partial t} C(q,t) = -\frac{1}{A_0} \frac{\partial}{\partial q} \int_{q^* \leq q} D \nabla^2 q^* dS \quad (4)$$

where  $D$  is the diffusivity. Nakamura (1996) developed the effective diffusivity method by focusing on the RHS of the equation and by introducing the equivalent length. Here we propose a new method by utilizing the LHS of the equation, i.e. the term  $\frac{\partial}{\partial t} C(q,t)$ .

By definition  $C(q,t)$  is between 0 and 1, and the change in the shape of the curve  $C(q,t)$

as a function of  $q$  is entirely due to the diffusion when no sources or sinks of the tracer exist in the domain. Subsequently, the area enclosed by the two  $C(q,t)$  curves at adjacent time steps ( $t$  and  $t+\delta t$ , with  $\delta t \rightarrow 0$ ) on  $q/(q_{\max} - q_{\min})$  -  $C$  plane is:

$$\frac{1}{q_{\max} - q_{\min}} \int_{q_{\min}}^{q_{\max}} \left| \frac{\partial}{\partial t} C(q,t) \right| dq = \frac{1}{A_0 (q_{\max} - q_{\min})} \int_{q_{\min}}^{q_{\max}} \left| \frac{\partial}{\partial q} \int_{q^* \leq q} D \nabla^2 q^* dS \right| dq \quad (5)$$

or equally

$$\int_0^1 \left| \frac{\partial}{\partial t} C(\tilde{q},t) \right| d\tilde{q} = \frac{1}{A_0} \int_0^1 \left| \frac{\partial}{\partial \tilde{q}} \int_{\tilde{q}^* \leq \tilde{q}} D \nabla^2 \tilde{q}^* dS \right| d\tilde{q} \quad (6)$$

where  $\tilde{q} = (q - q_{\min}) / (q_{\max} - q_{\min})$  is the normalized tracer concentration. Therefore, the area change, as represented by the LHS of Eqs. (5) and (6), is one kind of measure for the mean intensity of eddy diffusion in the domain (RHS of Eqs. (5) and (6)).

Similar to the effective eddy diffusivity of Nakamura (1996), the CDF index is also a global, not local, measurement of the eddy diffusion because the area (CDF) for  $q$  has to be counted for all of  $q_* \leq q$  over the entire domain. To account for the patchiness of eddy-induced mixing in the Southern Ocean, we introduce here a localized or patchy CDF index by combining the forward and backward trajectory calculation with original CDF method.

Suppose a spatially fixed area  $\hat{A}$ , no matter its geometrical shape, is large enough to contain enough samples (grids) for the CDF to be meaningful. Because of the cross-boundary flow and transport, the CDF method cannot be applied directly to this limited and fixed area. However, during a short time period ( $\delta T$ ), the mass in the area is

composed of three subgroups: (1) the part remaining in the area and never crossing the boundary during the period; (2) the part initially being within the area, but flowing outside during the period; (3) the part initially being outside of the area, but flowing inside the area during the period. The mass in the second and third parts represents the mass transport and exchange between the fixed area and the outside. For a quasi non-divergent flow, the out-flow mass in part (2) should be close to equal to the in-flow mass in part (3). The tracer in part (1) of  $\hat{A}$  forms an isolated and closed subsystem if no source and sink exists, and the CDF method described above can be equally applicable to this closed subsystem. To isolate this closed system from  $\hat{A}$ , we need to exclude the mass in part (2) and part (3) from  $\hat{A}$ . We do this by calculating the forward trajectory (for part 2) and backward trajectory (for part 3). If the trajectory moves across the boundary of the limited area during the integration, then the initial (final) point for forward (backward) trajectory integration is excluded from the calculation of CDF. In our calculation, the CDF is counted by dividing the span for tracer concentration ( $q_{\min}, q_{\max}$ ) into 50 bins. The final CDF index is further divided by two, because the increase in CDF for a particular tracer concentration must be compensated by decrease in CDF for another tracer concentration and the area enclosed by the CDF curve on the  $\tilde{q}$ -CDF plane is conserved in the case that no sink/source exists for the tracer. In our calculation,  $\hat{A}$  is a 8-degree (zonal)  $\times$  3 degree (meridional) area centered at each model grid on which the CDF is calculated.

### *c. The Relative Dispersion Method and Finite Size Lyapunov Exponent*

The standard calculation of relative dispersion and relative diffusion depends on the statistics of a cloud of pairs (LaCasce, 2008). Due to the limitation of model

resolution, we define the relative dispersion as the ratio of pair separation after a finite time to the initial separation of the pair. Four pairs are used at each model grid, with one particle of the pair on the grid and the other on one of its four neighboring model grids, i.e. the initial separation for the pairs is 1/6 degrees. In our calculation, the time for integration in calculating the relative dispersion is 30 days, mainly based on the time scale of eddies and initial pair separation. The initial particles are seeded repeatedly at 5-day intervals. The final results are the time mean over the 2 years of the SOSE reanalysis.

The Finite Size Lyapunov Exponent (FSLE) is also calculated based on the trajectories by using the method as in d’Ovidio *et al.* (2004). The initial separation is 1/6 degree, the model resolution, and the final distance is 2 degrees.

The trajectories used for CDF, relative dispersion and FSLE are computed by integrating the isopycnally projected zonal and meridional velocities on isopycnal levels with a fourth order Runge-Kutta scheme with a fixed time step of 1 day.

#### *d. Ocean Reanalysis*

We use the results from Southern Ocean State Estimate (SOSE, Mazloff *et al.*, 2009) derived from observations over the period 2005-2006. SOSE is an assimilation of ocean observations with the MITgcm, a 1/6 degree eddy permitting model. The ocean observations assimilated in SOSE include data from CTD synoptic sections, hydrographic climatology, satellite altimetry, and XBTs. Mazloff *et al.* (2009) showed that the overall structure of the ACC is reasonably well represented in the SOSE. The original SOSE is on 42 depth (z) levels ranging from near surface to more than 5000 m

depth. We project the velocity fields to 20 potential density (isopycnal) surfaces ranging from  $26 \text{ kg/m}^3$  to  $27.85 \text{ kg/m}^3$ .

Ertel's Potential vorticity (PV) is used as the tracer concentration in diagnosing the eddy mixing. PV in its approximate form is calculated:

$$P = -f \frac{\partial \sigma}{\rho \partial z} \quad (7)$$

where  $\sigma$  is the potential density,  $f$  is the Coriolis parameter, and  $\rho$  the density. A check revealed that the contribution of relative vorticity to PV is small. To minimize the possible error in interpolation to isopycnal surfaces, we calculate PV first in the original depth coordinate and then interpolate PV to the target isopycnal surfaces. Vertical profiles are mapped back onto the depth coordinate using the mean depths of the isopycnal surfaces.

### 3. Comparison of the methods

Next, we compare the four methods in describing the spatial structure of isopycnal mixing, using the measures  $M_e$ , CDF, relative dispersion, and FSLE on an intermediate isopycnal (potential density) surface  $\sigma=27.7 \text{ kg/m}^3$  (Figure 2). There are important differences between the four measures but we first provide a general overview. We see enhanced mixing in the Agulhas Current System to the south of Africa and along the mid-ocean ridge; there are enhanced mixing zones to the north of the Kerguelen Plateau near 70E, to the south of Australia, and near the Campbell Plateau south of New Zealand. In the southern Pacific, the enhanced mixing areas are clearly related to the

Pacific Antarctic Ridge and to the fracture zones. Then the mixing is enhanced again in the Drake Passage, and in the western boundary current in the Southwestern Atlantic. The large values of the CDF (Fig. 2b) in the Weddell Sea Gyre area and a few areas close to the Antarctic continent are mainly due to strong nonconservative processes in the model in these regions, partly related to convection, and are not considered further here.

Because both the relative dispersion (Fig. 2c) and the FSLE (Fig. 2d) are based on the calculation of Lagrangian trajectories, it is not surprising that they show similar spatial structure. The enhanced dispersion and FSLE are found in the Agulhas Retroflection north of the ACC, to the northward and down-stream side of the Kerguelen Plateau, to the east end of the Southeast Indian Ridge (about 150E), over the Pacific Antarctic Ridge and the fracture zones, to the east of the Drake Passage, and in the Brazil Current area.

The vertical structure of isopycnal mixing according to the four methods shows key differences (Fig. 3). While both relative dispersion and FSLE monotonically decay with the depth, the profiles of  $M_e$  and CDF show enhanced mixing in the depth range of 1500-2500 m. The mid-depth enhancement is evident to the north of the Southwest Indian Ridge and underneath the large Agulhas EKE center, though the vertical structures of  $M_e$  and CDF are different in the Agulhas Current System. Due to the limitation of time-resolution and also due to the assimilation procedure, the calculation of CDF, which is based on the statistics of the tendency term at intervals of 5 days, may involve more random or computational errors than the merely time-averaged statistics such as  $M_e$ . Given the difference shown in Figure 3 between  $M_e$  and CDF, we find by calculating the pattern correlation of the mixing indices (Fig. 4a) between 35S and 65S that the pattern

correlation between CDF and  $M_e$  is significant, though not as high as between FSLE and dispersion. In addition, Figure 4a shows that the correlations between CDF with FSLE and dispersion at mid-depth are much lower, suggesting their essential disagreement.

The difference of the indices can also be seen in their relation with the square root of EKE ( $\sqrt{EKE}$ ). Figure 2 suggests that both the relative dispersion and the FSLE closely follow the distribution of EKE, consistent with Stammer (1998) among many others. Figure 4b further shows that the pattern correlations of relative dispersion and FSLE with the  $\sqrt{EKE}$  reach 0.8-0.9 on each isopycnal surface. However, compared with relative dispersion and FSLE, the correlations of  $M_e$  and CDF with the  $\sqrt{EKE}$  at mid- and upper layers are relatively low, though at deep layers the correlations are much larger.

The difference in both horizontal and vertical structures of the eddy mixing or diffusion based on the  $M_e$  (or CDF) methodology compared to the relative dispersion (or FSLE) methodology results, we think, from both the detailed space and time averaging of the methods, and from the relationship of this averaging to the mean fields. While the mathematical description of turbulent dispersion based on Taylor's (1921) isotropic theory has long been established (e.g. Garrett, 2006; LaCasce, 2008), it has been noted that the assumption of stationary and spatially homogeneous mean flow is almost certainly not suitable for the majority of the ocean. The role of jets as barriers or amplifiers for mixing is not as clear from the relative dispersion or FSLE viewpoint as from the  $M_e$  or CDF viewpoint, because these latter methods, especially the CDF, more readily follow the evolution of the tracer itself, naturally distinguishing regions of greater

and lesser mixing. Subtropical jets in the stratosphere, for example, have large FSLE, but are thought to act as transport barriers (d’Ovidio *et al.*, 2009). Because of the difficulty in defining the mean flow, shear dispersion or stretching, is to some extent, included in the Lagrangian-based relative dispersion and also in the FSLE.

Just how closely the  $M_e$  and CDF methods represent irreversible mixing of tracers is not well determined, but Nakamura (2001) has shown the  $M_e$  method to be useful in the atmospheric context. The CDF method in particular is theoretically consistent with the Nakamura’s effective diffusivity (Nakamura, 1996; Nakamura, 2008). Although both CDF and  $M_e$  may be problematic in the upper few hundreds of meters of the ocean where diabatic processes prevail and their spatial pattern exist differences, the correlation between CDF and  $M_e$  in Figure 4a supports to some extent the idea that  $M_e$  is relevant to the irreversible mixing in the ocean. In the deep ocean, the four indices are basically similar to each other, possibly due to a much weaker mean current. We note, however, that the low time resolution of ocean reanalysis may cause more errors in the calculation of CDF, which involves the calculation of both trajectories and tendency, than in  $M_e$ , which only involves the spatial-temporal averaging of PV gradients. Therefore, we will focus mainly on  $M_e$  as a proxy of irreversible isopycnal mixing and explore its relations with jets and topography in the following sections.

## 4. Jets and the vertical structure of mixing

Marshall *et al.* (2006) suggest that the eddy-induced surface mixing is large on the equatorial flank of the ACC and is smaller at the jet core. By calculating the linearly unstable baroclinic modes, Smith and Marshall (2009) propose that the critical layer or

steering level is responsible for the enhanced mixing both on the equatorial flank of jet core of the ACC at the mixed layer and at the depth of about 1000m just under the jet core. Based on mixing length scales determined from hydrographic data analysis, Naveira-Garabato *et al.* (2009) suggest that jets or fronts in the ACC tend to suppress mixing according to the mixing length theory proposed by Ferrari and Nikurashin (2010). Here we will show that our calculation also suggests the jets act as partial barriers to mixing at mid-depth, while under the ACC jet cores eddy mixing is enhanced.

By mapping potential density surfaces back to the depth coordinate, we find for most of the ACC system that the latitude of jet cores at 1000m is close to the latitude of maximum meridional PV gradient (Fig. 5a), suggesting that the jet cores still work as an impediment to mixing 1000m depth; the areas of relatively strong mixing ( $M_e$ , Fig. 5b) are located on the northern flank of jet cores. However, for isopycnal surfaces near 1550m depth (Fig. 5c,d), most of the enhanced mixing is located close to the jet cores and is associated with weak PV gradients.

The mean depth (1500-2000m) for the maximum  $M_e$  in the ACC is larger by about 1000m than the steering depth in Smith and Marshall (2009). That steering depth was based on observed propagation in the ACC and a linear wave analysis, but identifying propagation in the ACC as linear waves is problematic. Chelton *et al.* (2007) suggest that most of the observed propagation speed of eddies in altimetric data is the displacement of nonlinear eddies, rather than the propagation of linear Rossby waves (Chelton and Schlax, 1996). Smith and Marshall (2009) show that in nonlinear simulations with an evolving mean state, the steering level is deeper, moving from about 1000m to 1600m, more in line with our results, and the scale of the fastest growing eddy

is about 40 km, which is closer to the observed eddy scale. Abernathey et al. (2010), also using SOSE, show deeper penetration as well but attribute this again to steering level effects. We suggest, in the next section, that topography is an important factor responsible for the deeper eddy-induced mixing.

## 5. Topography and enhanced eddy mixing

We focus on the enhanced mid-depth isopycnal mixing which is robust in both  $M_e$  and CDF methods, and the apparent relation with topography in the Southern Ocean. Figure 5d (see also Fig.1) shows that larger deep mixing values are generally associated with stronger flow, where it intersects topography, qualitatively suggesting that the enhancement of mixing may be related to the main bathymetric features. For descriptive purposes only, we refer to this as a topographic localization. Aside from higher  $M_e$  in the Agulhas Retroflection, key areas of mixing appear where the main fronts cross the mid-ocean ridge near 30 E, 70-80 E, 150 E, and 150 W. The Drake Passage region near 60 W is also one where the fronts cross ridges, but also one where PV gradients are large and elevated mixing is less clearly concentrated.

Figure 6 shows the PDFs of the mean current speed that is associated with strong mixing ( $\log_{10} M_e > 1$ , binned at 1 cm/s intervals). They have been normalized relative to the total number of grid points in the corresponding ensemble, and it should be noted first that the topographic localization of isopycnal mixing is evident by the number (about 20,000) of points with strong mixing in the topography-related ensemble, much larger than its counterpart (about 4,300) in the non-topography-related ensemble. Thus, there is a much greater volume of the ocean associated with the strong mixing localized to

topography. The PDFs are calculated for an ensemble of four meridional slices, of 2 degrees zonal width, centered at 30E, 70E, 80 E and 150W for the topography group, and for another ensemble of four meridional slices centered at 110E, 115E, 110W, and 30W with no dominating topographic structure. Both ensembles have a similar number of grid points, that is, about 120,000 within the 900-2800m depth range. The most common speed associated with strong mixing is, interestingly, 2-3 cm/s both near and away from the selected topography; however, the topographic peak is broader, and we can see that strong mixing occurs more often in the topography-related ensemble at larger speeds. If the peaks (Fig. 6) suggest roughly the presence of critical levels in this depth range, the difference between the curves suggests that this effect is not dominant.

In the streamwise-averaged estimate of effective diffusivity, Abernathey *et al.* (2010) find enhanced mixing beneath the single jet core of the ACC but rising toward the surface on the equatorward flank (see their Fig. 4). However, the streamwise averaging method smooths over multiple jets and neglects the local, detailed nature of the mixing. Next, we illustrate with more detail the 3D structure of the localized eddy mixing and how the mid-depth enhancement of mixing is closely related to the topography in the ACC (Figs. 7-10).

In the Atlantic – Indian Ocean sector between 0 and 60E, the main bathymetric features are the Southwest Indian Ridge and plateaus (Agulhas and Crozet Plateaus), (Fig. 7a). The streamlines enveloped by the mean current speed isotachs (8cm/s, 6cm/s, and 4 cm/s in Figs. 7b, c, d, respectively) sketch out the fine and rich structure of the multiple jets in this part of the ACC. While the forcing of the ACC occurs mainly at the large scales of the wind field and buoyancy fluxes, we see that the smaller scale structure

of the fronts, such as splitting, merging, and meandering, follows to a great extent the shape of the topography. These deformations in the jets are present in the upper layers as well, for instance on the isopycnal surface  $27.5 \text{ kg/m}^3$  (Fig. 7b) which rises shallower than 1000m-depth at the location of the jets.

We find that on the  $27.5 \text{ kg/m}^3$  surface the mixing is weak in the core of the ACC jets. Though this is consistent with the effective diffusivity in Abernathey *et al.* (2010, their Fig. 6a), we should note that the reliability of  $M_e$  at shallow layers needs to be verified. The enhanced mixing on the  $27.5 \text{ kg/m}^3$  surface is mainly located in the Agulhas Current system and downstream where the mean depth of the surface is about 1500m. On the  $27.7 \text{ kg/m}^3$  surface (Fig. 7c), we see that the mixing in the Agulhas Current system is weakened, and that the spatial pattern of the enhanced mixing follows the east end of the Southwestern Indian Ridge and the northern branches of the ACC jets. Figure 7d shows more clearly the enhanced mixing near 2000m depth following the core of the ACC jets.

The jet at the northern flank of the Kerguelen Plateau (Figs. 8a-d) flows southeastward, merges with the narrow northeastward jet through the trough in the middle of the Kerguelen Plateau, and then splits to form jets flowing along the flank of the ridge. The mid-depth enhancement of eddy mixing (Figs. 8c-d) mainly follows the jets at the northern flank and the downstream wake of the Kerguelen Plateau.

The shape of the mid-ocean ridge and fracture zones south of Australia and the Campbell Plateau south of New Zealand (Fig. 9a) results in a complicated twisting of the jets between 145E and 165E (Fig. 9b-d). The twisted jets split into two branches: in the northern branch one single jet meanders northeastward along the southern edge of the

Campbell Plateau, and in the southern branch multiple jets move southeastward and then turn northeastward along the Pacific ridge flank. The two sets of jets merge at the fracture zones at about 140W in the Southern Pacific. In the upper layers at isopycnal depths of about 1000m or less, we find little enhanced mixing west of 180E even though the jets show strong twisting or curvature. Again, though the suppression of eddy mixing by the jets at upper layers seems consistent with Abernathey *et al.* (2010) and Ferrari and Nikurashin (2010), further verification is still needed. The mid-depth enhancement of eddy mixing is more closely linked to the twisted jets.

The shapes of multiple jets and the spatial pattern of strong mixing are constrained by flow through the Drake Passage to the South Atlantic (Fig. 10b-d). We see enhanced mixing associated more with the Malvinas Current (Fig. 10 b-d) than the Drake Passage flow at mid-depth, but an increase at about 3000m depth in the Drake Passage.

In summary, the mid-depth enhancement of eddy mixing tends to be associated with the interaction of the ACC and topography, and the merging of multiple jets embedded in the ACC. Both the mid-depth enhancement of eddy mixing by critical layers (Marshall *et al.*, 2006) and the regulation of mixing length scale by the presence of mean flow (Ferrari and Nikurashin, 2010) obtain with or without direct topographic influence, and do not take the role of topography and the multiple jets with fine spatial structures into consideration. Thompson (2010) analyzes the scale- and shape-dependence of the role of topography in eddy transport and mixing, and finds that the whole structure of mixing is itself a complex dynamical phenomenon, even over relatively smooth topography. The bending, splitting, merging, etc. in the presence of topography may

narrow the scale of time-mean jets. We emphasize also the discontinuous nature of the jets, as the flow broadens or concentrates over diverse topographic slopes. This can make the propagation of eddies much more complicated than assumed in the simplified theoretical arguments. Rhines (1989, 2007) suggests a somewhat more generalized framework, in which the wake structure associated with topography may induce PV mixing through instability and near-zero phase speed of Rossby wave propagation.

It is difficult to synthesize the behavior of the multiple jets in the ACC (Figs. 7-10), but it seems that the merging or convergence of the jets does more to induce the mid-depth enhancement of mixing than the splitting of the jets does. Merging moreover results in the interruption of the downstream propagation of eddies and collisions. As an example, the Hovmöller diagram in Figure 11a shows eddies propagating eastward along 51S, but the propagation is interrupted by the eddies with opposite sign at about 28-30E. At this location several branches of the ACC converge to flow a passage in the Southwest Indian Ridge. There, the jets interact with southward propagating eddies (Fig. 11b) and deep mixing (Fig. 7d) increases. The interaction of barotropic and baroclinic eddies is strong over topography (e.g. Witter and Chelton, 1998) and this interaction seems to be producing stronger eddy mixing with a sharper vertical structure. Our diagnostics presently do not identify the dominant mechanisms, however.

## 6. Conclusions and discussion

We develop a localized cumulative probability density function (CDF) method in conjunction with the calculation of forward and backward Lagrangian trajectories from an ocean reanalysis. The new method suggests the applicability of Nakamura's (2001)

mixing efficiency ( $M_e$ ) representing the localized and patchy eddy-induced mixing in the oceans. Note that in principal the forward and backward Lagrangian trajectories can equally be applied to Nakamura's effective diffusivity method (Nakamura, 1996; Shuckburgh and Haynes, 2003; Marshall *et al.*, 2006) for describing the patchy nature of eddy mixing.

The calculation of  $M_e$  and CDF from the SOSE is consistent with the notion that jets generally act as zones of reduced mixing above about 1000m depth, but that this breaks down at mid-depths, where both the  $M_e$  and CDF methods reveal a prevailing mid-depth enhancement of mixing in the Southern Ocean.

We also examine the relative dispersion and Finite Size Lyapounov Exponent (FSLE) and find the distribution of dispersion and FSLE in the Southern Ocean follows fairly closely the 3D structure of eddy kinetic energy (EKE). Comparison of the four methods shows that relative dispersion and FSLE may have limitations in reflecting the role of jets as mixing barriers, possibly due to the difficulty in specifying the mean flow. The  $M_e$  and CDF methods may be more suitable for approaching an estimate of irreversible eddy-induced mixing in the ocean, though either of these two methods may suffer from nonconservative processes near boundaries.

Topography strongly shapes the spatial structure of flow and eddy mixing in the Southern Ocean, and generally appears to enhance the eddy mixing under some conditions. The mean current speeds at which mixing is strongest, are generally larger and more scattered in the cases with topography than in the cases with no topography.

The mid-depth enhancement of eddy mixing seems to be associated with the interaction of topography and multiple jets embedded in the ACC.

While our diagnosis leads us to suggest that topography plays a fundamental role in enhancing mixing and expanding the mid-depth eddy-mixing in the Southern Ocean, the mechanism for this influence on the vertical structure of mixing is not clear. Preliminary analysis suggests enhanced eddy mixing over topography is, in places, due to locally enhanced baroclinicity and instability within the wake, itself at least partly due to the mean convergence of eddies in merging branches of the ACC. Interaction of barotropic and baroclinic eddies (e.g. Witter and Chelton, 1998) may be important to setting the greater strength and vertical structure of eddy mixing associated with topography. Detailed analysis of these mechanisms is underway.

Eddy mixing and diffusivity is thought to be essential in setting the strength of transport by ACC and of the overturning circulation. Moreover, the wind stress and bottom form stress are linked by the vertical transport of horizontal momentum through interfacial eddy-related form drag (see review by Rintoul *et al.*, 2001). The local and patchy nature of eddy mixing and diffusivity may imply that locally the vertical transport of momentum is channeled into patchy zones with strong eddy mixing. To address this, a detailed analysis of the relationship between eddy mixing and the 3D structure of form stress was performed but without clear conclusions; nevertheless, this direction may lead to a better understanding of the link between eddies and large-scale circulation in the ACC.

Finally, the methods developed or adopted here mainly give qualitative pictures of the pattern of eddy mixing. Due to the limitations of both the ocean reanalysis and the methods themselves, the spatial patterns of eddy mixing in the  $M_e$  and CDF methods still show important differences relative to each other. Nonlocal effects and the simplifications inherent in  $M_e$  may also play a role. Thus, additional verification with assimilated data, observations and model simulations at higher resolution is needed.

## 7. Acknowledgements

The authors thank Matt Mazloff at SIO at UC San Diego for providing the SOSE data and assistance in using the data. SOSE was supported by the National Science Foundation through TeraGrid resources provided by Texas Advanced Computing Center under grant number MCA06N007. We are also grateful to two anonymous reviewers and the editor for their constructive and insightful comments. The research is supported by NSF grant OCE 0927583. This is Geophysical Fluid Dynamics Institute contribution No. 464.

## References

- Abernathay, R., J. Marshall, M. Mazloff and E. Shuckburgh. 2010. Enhancement of mesoscale eddy stirring at steering levels in the Southern Ocean. *J. Phys. Oceanogr.*, *40*, 170-184.
- Boss, E. and L. Thompson. 1999. Lagrangian and tracer evolution in the vicinity of an unstable jet. *J. Phys. Oceanogr.*, *29*, 288-303.
- Bower, A. S. 1991. A simple kinematic mechanism for mixing fluid parcels across a meandering jet. *J. Phys. Oceanogr.*, *21*, 173-180.
- Bower, A. S. and M. S. Lozier. 1994. A closer look at particle exchange in the Gulf Stream. *J. Phys. Oceanogr.*, *24*, 1399-1418.
- Chelton, D. B. and M. G. Schlax, 1996. Global observations of oceanic Rossby waves. *Science*, *272*, 234-238.
- Chelton, D. B., M. G. Schlax, R. M. Samelson and R. A. de Szoeke. 2007. Global observations of large oceanic eddies. *Geophys. Res. Lett.*, *34*, doi:10.1029/2007GL030812.
- d'Ovidio, F., V. Fernández, E. Hernández-García and C. López. 2004. Mixing structures in the Mediterranean from finite-size Lyapunov exponents. *Geophys. Res. Lett.*, *31*, L17203, doi:10.1029/2004GL020328.
- d'Ovidio, F., E. Schuckburgh and B. Legras, 2009. Local mixing events in the upper-troposphere lower-stratosphere: Part 1, detection with Lyapunov diffusivity. *J. Atmos. Sci.*, doi:10.1175/2009JAS2982.1.
- Ferrari, R. and M. Nikurashin. 2010. Suppression of eddy diffusivity across jets in the Southern Ocean. *J. Phys. Oceanogr.*, *40*, 1501-1519.

- Garrett, C. 2006. Turbulent dispersion in the ocean. *Prog. Oceanogr.*, *70*, 113-125.
- Griesel, A., S. T. Gille, J. Sprintall, J. L. McClean, J. H. LaCasce, and M. E. Maltrud (2010), Isopycnal diffusivities in the Antarctic Circumpolar Current inferred from Lagrangian floats in an eddying model, *J. Geophys. Res.*, *115*, C06006, doi:10.1029/2009JC005821.
- Hughes, C. W. and E. R. Ash. 2001. Eddy forcing of the mean flow in the Southern Ocean. *J. Geophys. Res.*, *106C2*, 2713-2722.
- Joseph, B. and B. Legras. 2002. Relation between kinematic boundaries, stirring, and barriers for the Antarctic polar vortex, *J. Atmos. Sci.*, *59*, 1198-1212.
- LaCasce, J. H. 2008. Statistics from Lagrangian observations. *Prog. Oceanogr.*, *77*, 1-29.
- Lindzen, R. S. 1993. Baroclinic neutrality and the tropopause. *J. Atm. Sci.*, *50*, 1148-1151.
- Lozier, M. S. and D. Bercovici. 1992. Particle exchange in an unstable jet. *J. Phys. Oceanogr.*, *22*, 1506-1516.
- Lozier, M. S., L. J. Pratt, A. M. Rogerson and P. D. Miller. 1997: Exchange geometry revealed by float trajectories in the Gulf Stream. *J. Phys. Oceanogr.*, *27*, 2327-2341.
- MacCready P. and P. B. Rhines. 2001: Meridional transport across a zonal channel: topographic localization. *J. Phys. Oceanogr.*, *31*, 1427-1439.
- Marshall, D. 1995. Topographic steering of the Antarctic Circumpolar Current. *J. Phys. Oceanogr.*, *25*, 1636-1650.
- Marshall J., E. Shuckburgh, H. Jones and C. Hill, 2006. Estimates and Implications of surface eddy diffusivity in the Southern Ocean derived from tracer transport. *J. Phys. Oceanogr.*, *36*, 1806-1821.

- Mazloff, M. R., P. Heimbach and C. Wunsch, 2009. An eddy-permitting Southern Ocean state estimate. *J. Phys. Oceanogr.*, *40*, 880-899.
- Nakamura, M. and Y. Chao, 2001. Diagnoses of an eddy-resolving Atlantic ocean simulation in the vicinity of the Gulf Stream. Part I: Potential Vorticity. *J. Phys. Oceanogr.*, *31*, 353-378.
- Nakamura, N. 1996. Two-dimensional mixing, edge formation, and permeability diagnosed in an area coordinate. *J. Atmos. Sci.*, *53*, 1524-1537.
- Nakamura, N. 2001. A new look at eddy diffusivity as a mixing diagnostic. *J. Atmos. Sci.*, *58*, 3685-3701.
- Nakamura, N. 2008. Quantifying inhomogeneous, instantaneous, irreversible transport using passive tracer field as a coordinate, in J. B. Weiss and A. Provenzale eds., *Transport and mixing in geophysical flows. Lect. Notes Phys.*, *744*, Springer, Berlin, 137-164.
- Naveira-Garabato, A. C., R. Ferrari and K. L. Polzin. 2009. Eddy-induced mixing in the Southern Ocean. *J. Phys. Oceanogr.*, submitted.
- Orsi, A., T. Whitworth and W. Nowlin. 1995. On the meridional extent and fronts of the Antarctic Circumpolar Current. *Deep Sea Res. I*, *42*, 641– 673.
- Pierrehumbert, R. 1991. Large-scale horizontal mixing in planetary atmospheres. *Phys. Fluids A*, *3*, 1250-1260.
- Pratt, L. J., M. S. Lozier and N. Beliakova. 1995. Parcel trajectories in quasigeostrophic jets: Neutral modes. *J. Phys. Oceanogr.*, *25*, 1451-1466.
- Rhines, P. B. 1989. Deep planetary circulation and topography: simple models of midocean flows. *J. Phys. Oceanogr.*, *19*, 1449-1469.

- Rhines, P. B. 2007. Jets and orography: idealized experiments with tip jets and Lighthill blocking. *J. Atmos. Sci.*, *64*, 3627-3639.
- Rintoul, S. R., C. W. Hughes and D. Olbers. 2001. The Antarctic Circumpolar Current system, *in* Ocean Circulation and Climate, G. Siedler, J. Church, and J. Gould eds., Academic Press, New York, 271-302.
- Sallée, J.-B., K. Speer, R. Morrow and R. Lumpkin. 2008. An estimate of Lagrangian eddy statistics and diffusion in the mixed layer of the Southern Ocean. *J. Mar. Res.*, *66*, 441-463.
- Schuckburgh, E. and P. H. Haynes. 2003. Diagnosing tracer transport and mixing using a tracer-based coordinate system. *Phys. Fluids*, *15*, 3342-3357.
- Schuckburgh, E., H. Jones, J. Marshall and C. Hill. 2009. Understanding the regional variability of eddy diffusivity in the Pacific Sector of the Southern Ocean. *J. Phys. Oceanogr.*, *39*, 2011-2023.
- Stammer, D. 1998. On eddy characteristics, eddy transport, and mean flow properties. *J. Phys. Oceanogr.*, *28*, 727-739.
- Smith, K. S. and J. Marshall. 2009. Evidence for deep eddy mixing in the Southern Ocean. *J. Phys. Oceanogr.*, *39*, 50-69.
- Taylor, G. I. 1921. Diffusion by continuous movement. *Proc. London Math. Soc. Ser. A*, *20*, 196-221.
- Thompson, A. F. 2009. Jet formation and evolution in baroclinic turbulence with simple topography. *J. Phys. Oceanogr.*, doi:10.1175/2009JPO4218.1.
- Waugh, D.W. and E. R. Abraham. 2008. Stirring in the global surface ocean. *Geophys. Res. Lett.*, *35*, L20605, doi:10.1029/2008GL035526.

- Wiggins, S. 2005. The dynamical systems approach to Lagrangian transport in ocean flows. *Annu. Rev. Fluid Mech.*, 37, 295-328.
- Witter, D. L. and D. B. Chelton. 1998. Eddy-mean flow interaction in zonal oceanic jet flow along zonal ridge topography. *J. Phys. Oceanogr.*, 28, 2019-2039.

## List of Figures

Figure 1. Topography of the Southern Ocean. Red lines illustrate the hydrographic-based Polar Front and Subantarctic Front in the Southern Ocean (Orsi *et al.*, 1995). Grey shadings are the areas with mean current speed being no less than 15 cm/s (based on SOSE) at 55m depth.

Figure 2.  $\log_{10} M_e$ (a), CDF (b), relative dispersion (c), and FSLE (d) on the isopycnal surface  $\sigma=27.7 \text{ kg/m}^3$ . The black contours in (a) are mean depth of isopycnal surfaces; the black contours in (b)-(d) are contours of square root of eddy kinetic energy ( $\sqrt{EKE}$ ) larger than 6 cm/s, contour interval is 3 cm/s.

Figure 3. Meridional-vertical profiles (shaded) of  $\log_{10} M_e$ (a), CDF (b), relative dispersion (c), and FSLE (d) at 30E. Square root of eddy kinetic energy ( $\sqrt{EKE}$ ) is shown (white contours, interval 3 cm/s).

Figure 4. (a) Pattern correlations between the mixing indices: FSLE vs. relative dispersion (closed-square), and CDF vs  $\log_{10} M_e$  (closed-circle), relative dispersion (open circle), and FSLE (open square); (b) Pattern correlations between  $\sqrt{EKE}$  and the mixings indices: FSLE (closed square), relative dispersion (closed circle),  $\log_{10} M_e$  (open-circle), and CDF (open square). Correlation coefficients are calculated on the isopycnal surfaces over the ocean between 35S and 65S. The depth in the ordinate represents the mean depth of the isopycnal surfaces between 35S and 65S.

Figure 5. (a) Meridional PV gradient (shaded, units:  $10^{-15} \text{ m}^{-2} \text{ s}^{-1}$ ) and mean current speed (black contours, minimum at 6 cm/s with 3cm/s interval) at 1000m depth; (b)

Meridional PV gradient (shaded, units:  $10^{-15} \text{ m}^{-2} \text{ s}^{-1}$ ) and  $\log_{10} M_e$  (black contours, minimum of 0.8 with interval 0.2) at 1000m depth; (c) and (d) are the same as (a) and (b), but at 1550 m depth; in (c) the minimum mean current speed is 3 cm/s (black contour).

Figure 6. PDFs of mean current speed (binned by 1 cm/s interval), associated with strong mixing ( $\log_{10} M_e > 1$ ). The groups are sampled according to the relation to topography (see text). Samples from topographic areas (closed circle), or otherwise (open circle).

Figure 7. (a) Bathymetry (m) in the 0-60E sector of the Southern Ocean; (b) - (d) Streamline sketches at  $\sigma=27.5$  (b), 27.7 (c), and 27.8 (d)  $\text{kg/m}^3$  with enveloping red contour (8 cm/s for (b), 6 cm/s for (c), and 4 cm/s for (d)) of mean current speed. Blue shading represents the areas with the strong eddy mixing ( $\log_{10} M_e > 1$ ). Depth (1000m, 2000m, and 3000m) of the isopycnal surfaces is indicated (dashed lines).

Figure 8. The same as Fig. 7, but for the 60E-120E sector.

Figure 9. The same as Fig. 7, but for the 140E-120W sector.

Figure 10. The same as Fig. 7, but for the 100W-0W sector with the isopycnal surfaces in (b) and (c) at 27.6 and 27.75 kg/m<sup>3</sup>.

Figure 11. Hovmöller diagrams of the zonal component of current on the isopycnal surface  $\sigma=27.7$  kg/m<sup>3</sup> along 51S and 28E, respectively.

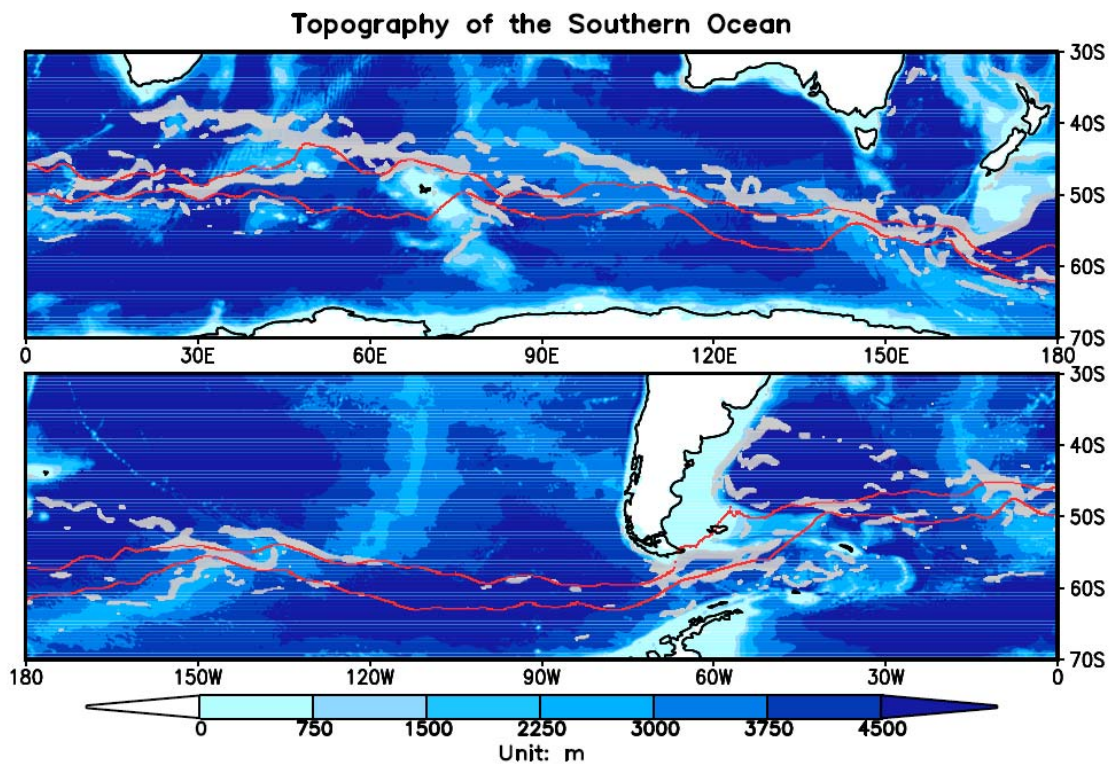


Figure 1. Topography of the Southern Ocean. Red lines illustrate the hydrographic-based Polar Front and Subantarctic Front in the Southern Ocean (Orsi *et al.*, 1995). Grey shadings are the areas with mean current speed being no less than 15 cm/s (based on SOSE) at 55m depth.

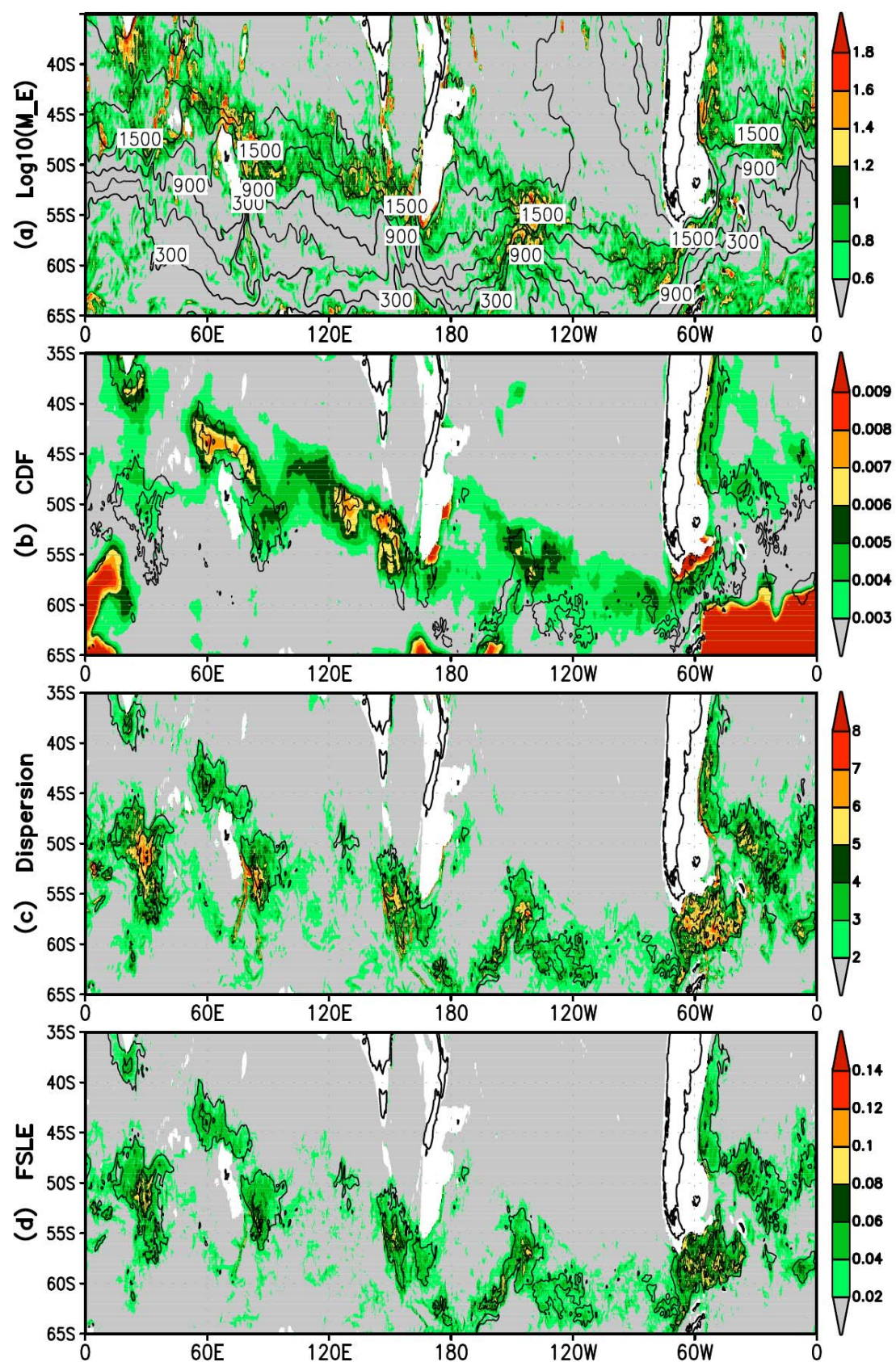


Figure 2.  $\log_{10} M_e$ (a), CDF (b), relative dispersion (c), and FSLE (d) on the isopycnal surface  $\sigma=27.7 \text{ kg/m}^3$ . The black contours in (a) are mean depth of isopycnal surfaces; the black contours in (b)-(d) are contours of square root of eddy kinetic energy ( $\sqrt{EKE}$ ) larger than 6 cm/s, contour interval is 3 cm/s.

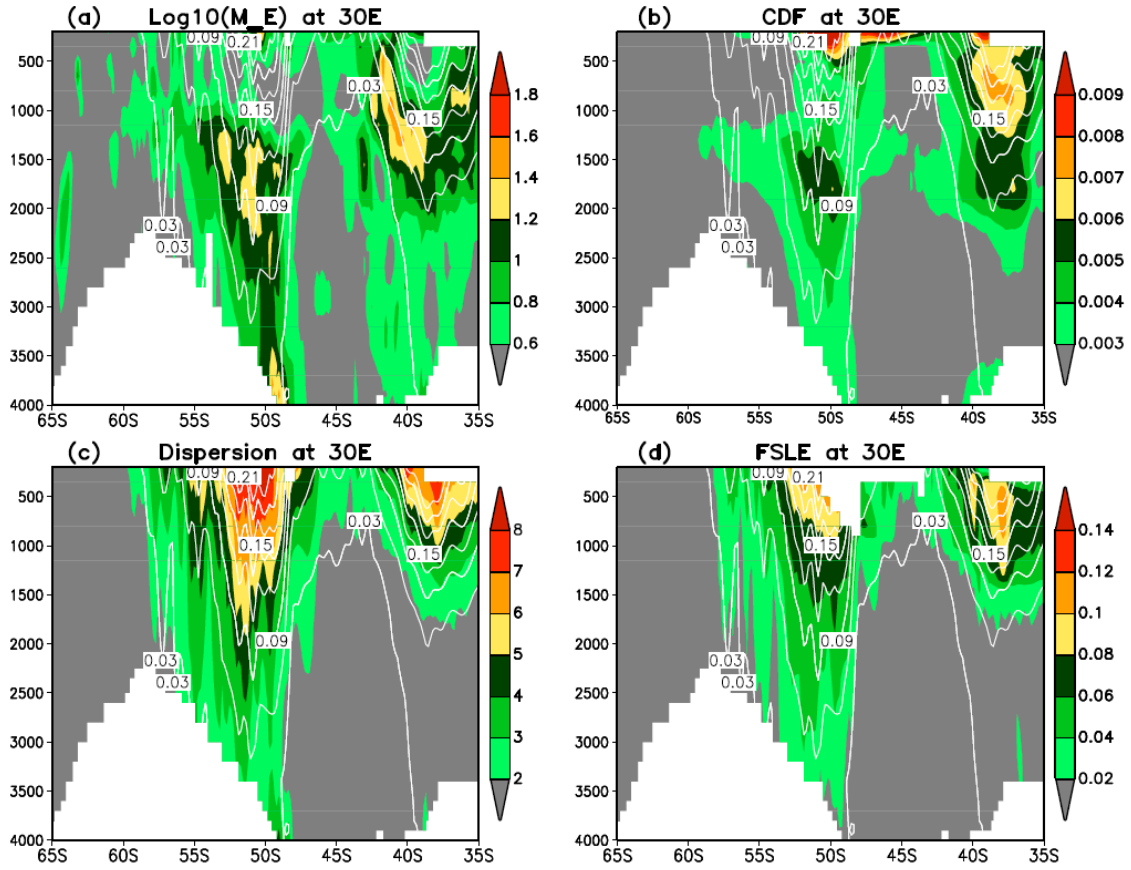


Figure 3. Meridional-vertical profiles (shaded) of  $\log_{10} M_e$  (a), CDF (b), relative dispersion (c), and FSLE (d) at 30E. Square root of eddy kinetic energy ( $\sqrt{EKE}$ ) is shown (white contours, interval as 3 cm/s).

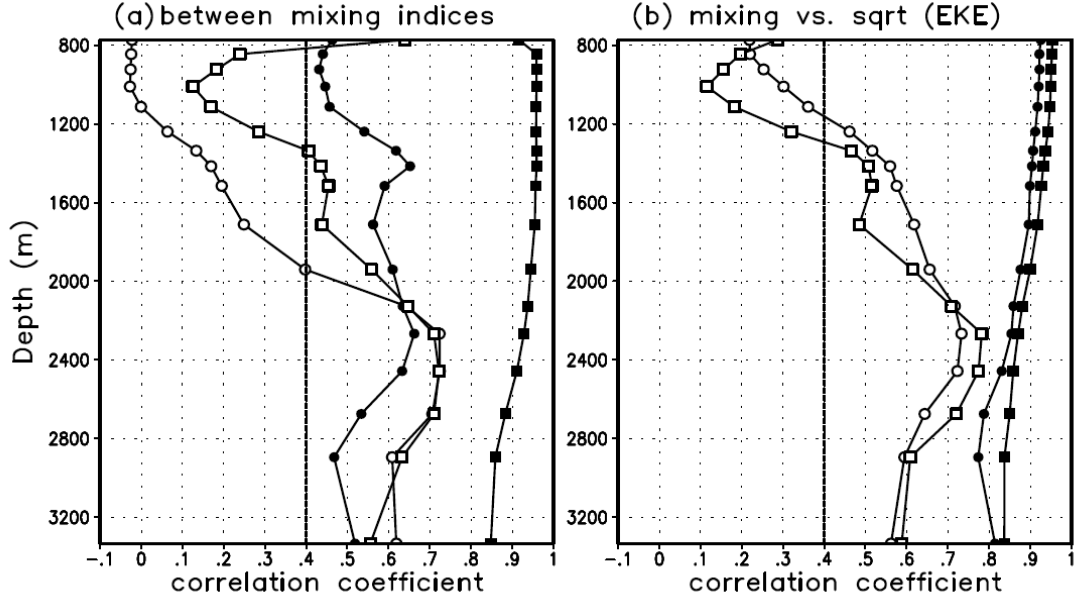


Figure 4. (a) Pattern correlations between the mixing indices: FSLE vs. relative dispersion (closed-square), and CDF vs  $\log_{10} M_e$  (closed-circle), relative dispersion (open circle), and FSLE (open square); (b) Pattern correlations between  $\sqrt{EKE}$  and the mixings indices: FSLE (closed square), relative dispersion (closed circle),  $\log_{10} M_e$  (open-circle), and CDF (open square). Correlation coefficients are calculated on the isopycnal surfaces over the ocean between 35S and 65S. The depth in the ordinate represents the mean depth of the isopycnal surfaces between 35S and 65S.

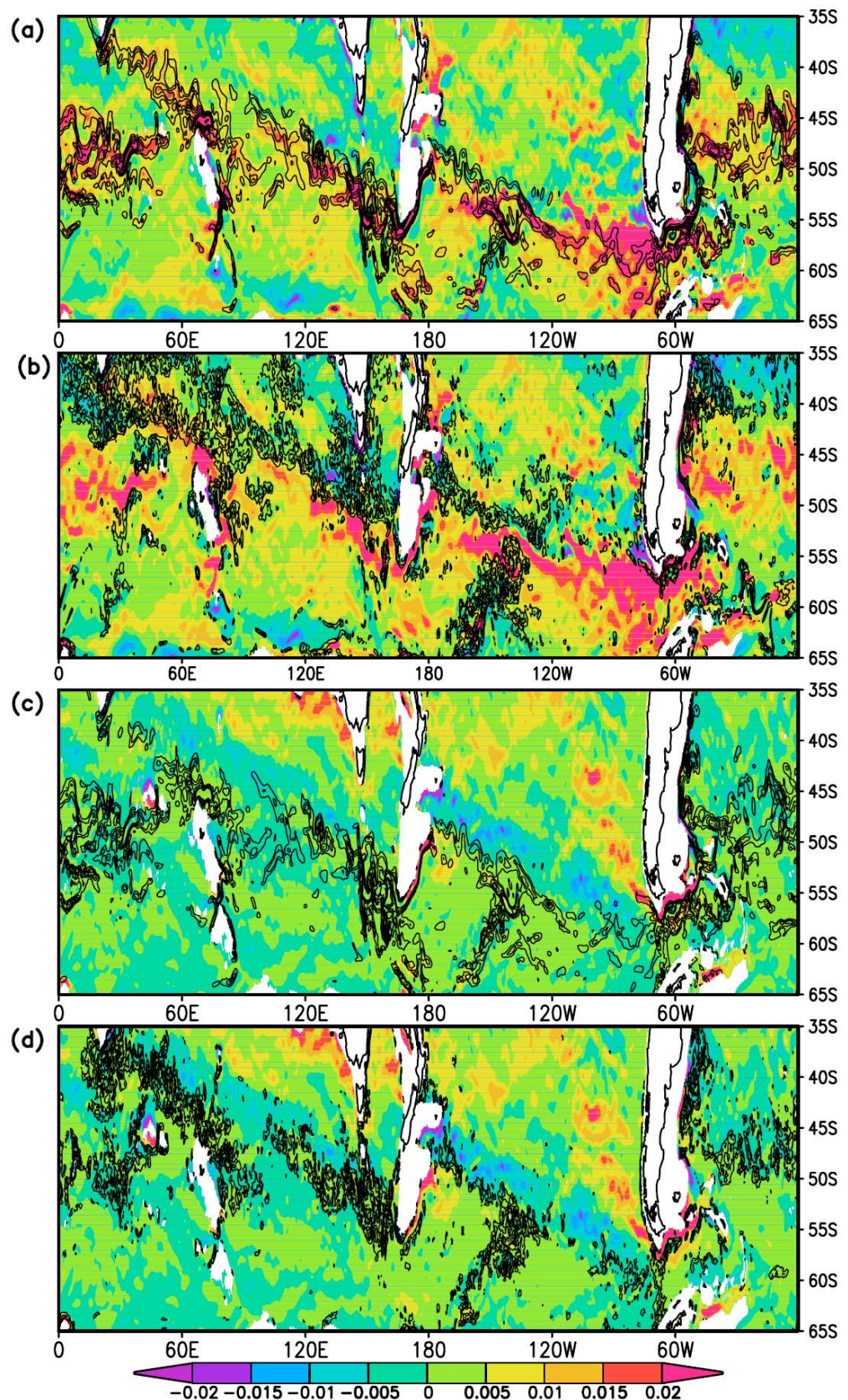


Figure 5. (a) Meridional PV gradient (shaded, units:  $10^{-15} \text{ m}^{-2} \text{ s}^{-1}$ ) and mean current speed (black contours, minimum at 6 cm/s with 3cm/s interval) at 1000m depth; (b) Meridional PV gradient (shaded, units:  $10^{-15} \text{ m}^{-2} \text{ s}^{-1}$ ) and  $\log_{10} M_e$  (black contours, minimum of 0.8 with interval 0.2) at 1000m depth; (c) and (d) are the same as (a) and (b), but at 1550 m depth; in (c) the minimum mean current speed is 3 cm/s (black contour).

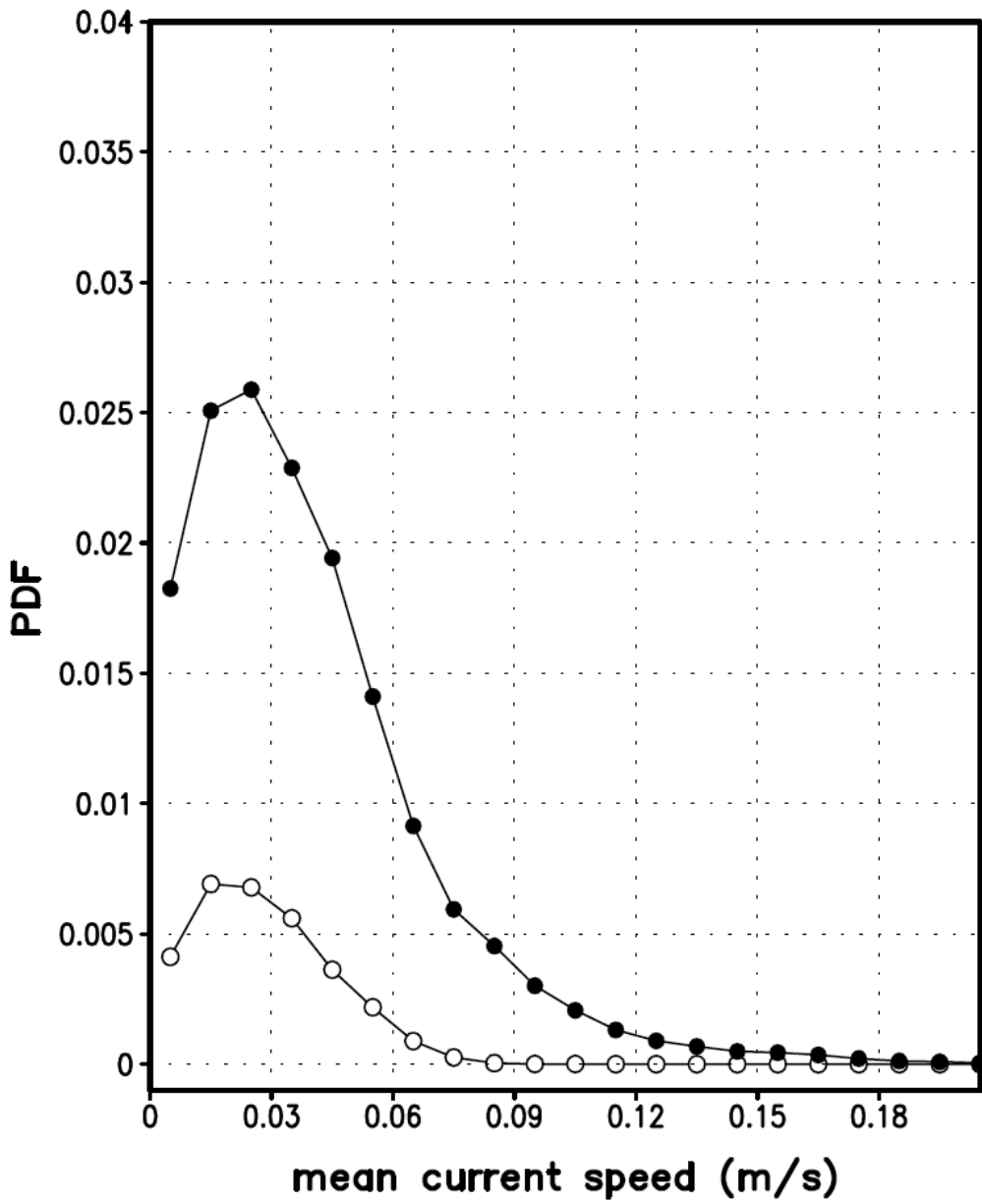


Figure 6. PDFs of mean current speed (binned by 1 cm/s interval), associated with strong mixing ( $\log_{10} M_e > 1$ ). The groups are sampled according to the relation to topography (see text). Samples from topographic areas (closed circle), or otherwise (open circle).

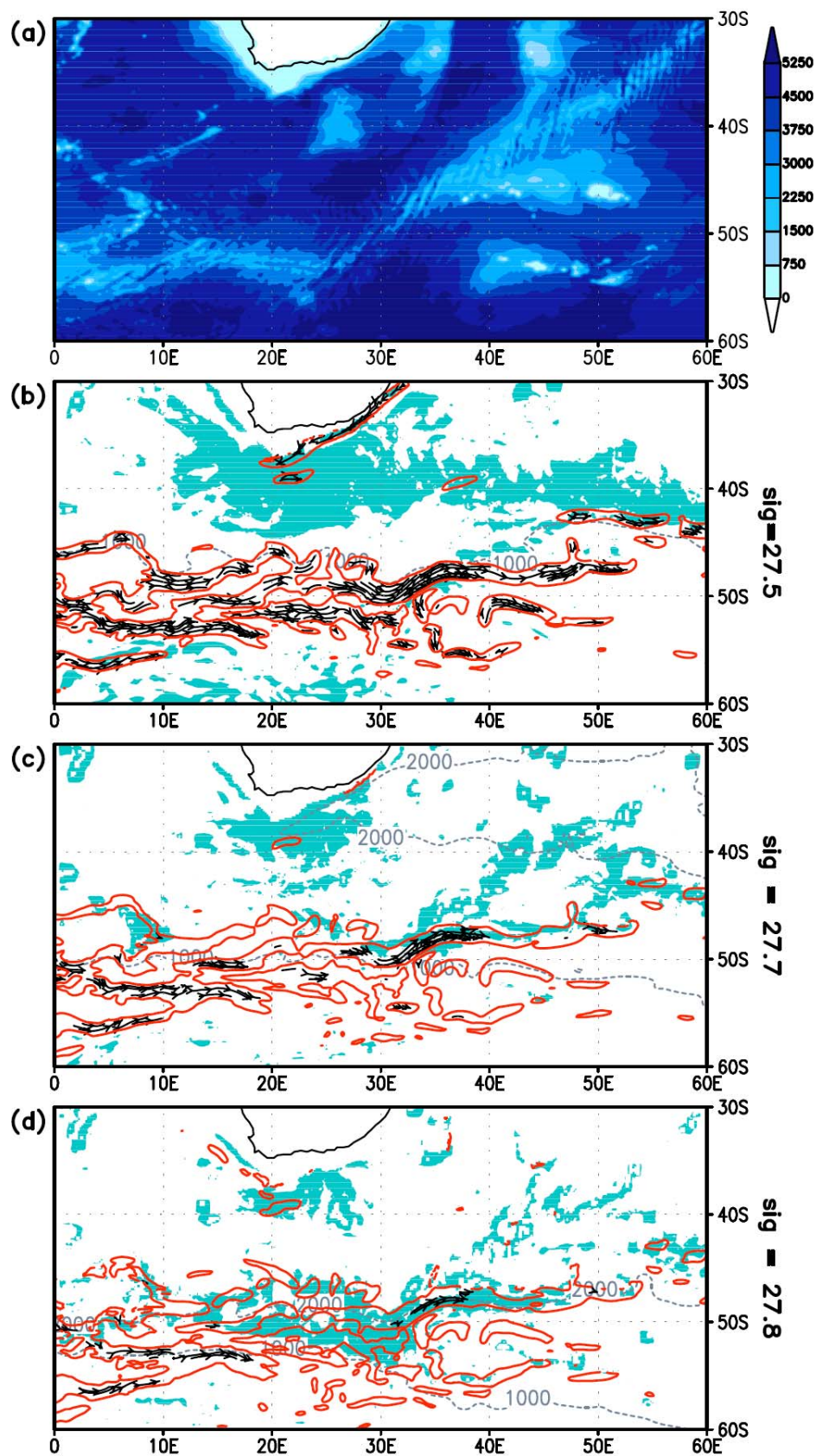


Figure 7. (a) Bathymetry (m) in the 0-60E sector of the Southern Ocean; (b) - (d) Streamline sketches at  $\sigma=27.5$  (b), 27.7 (c), and 27.8 (d)  $\text{kg/m}^3$  with enveloping red contour (8 cm/s for (b), 6 cm/s for (c), and 4 cm/s for (d)) of mean current speed. Blue shading represents the areas with the strong eddy mixing ( $\log_{10} M_e > 1$ ). Depth (1000m, 2000m, and 3000m) of the isopycnal surfaces is indicated (dashed lines).

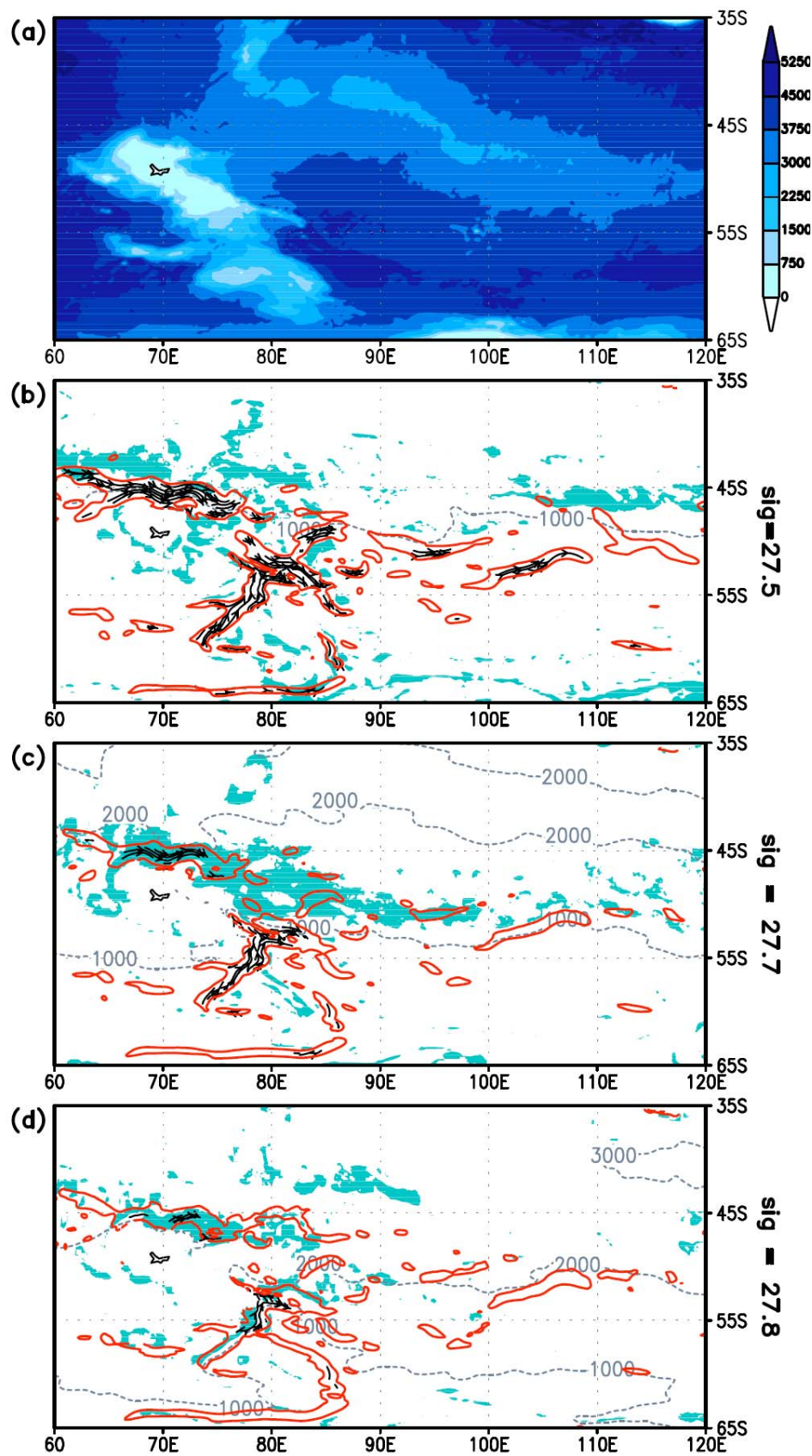


Figure 8. The same as Fig. 7, but for the 60E-120E sector.

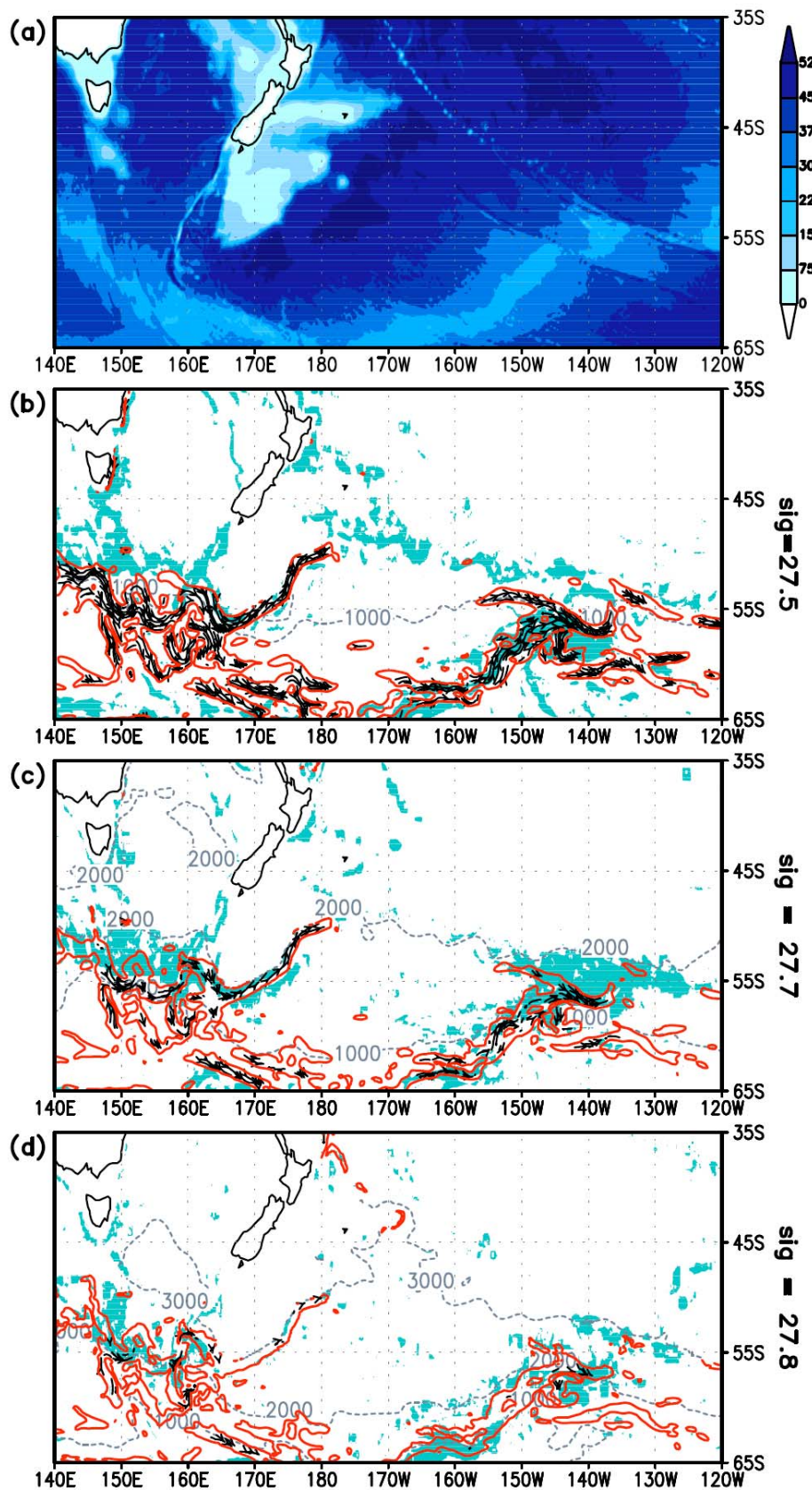


Figure 9. The same as Fig. 7, but for the 140E-120W sector.

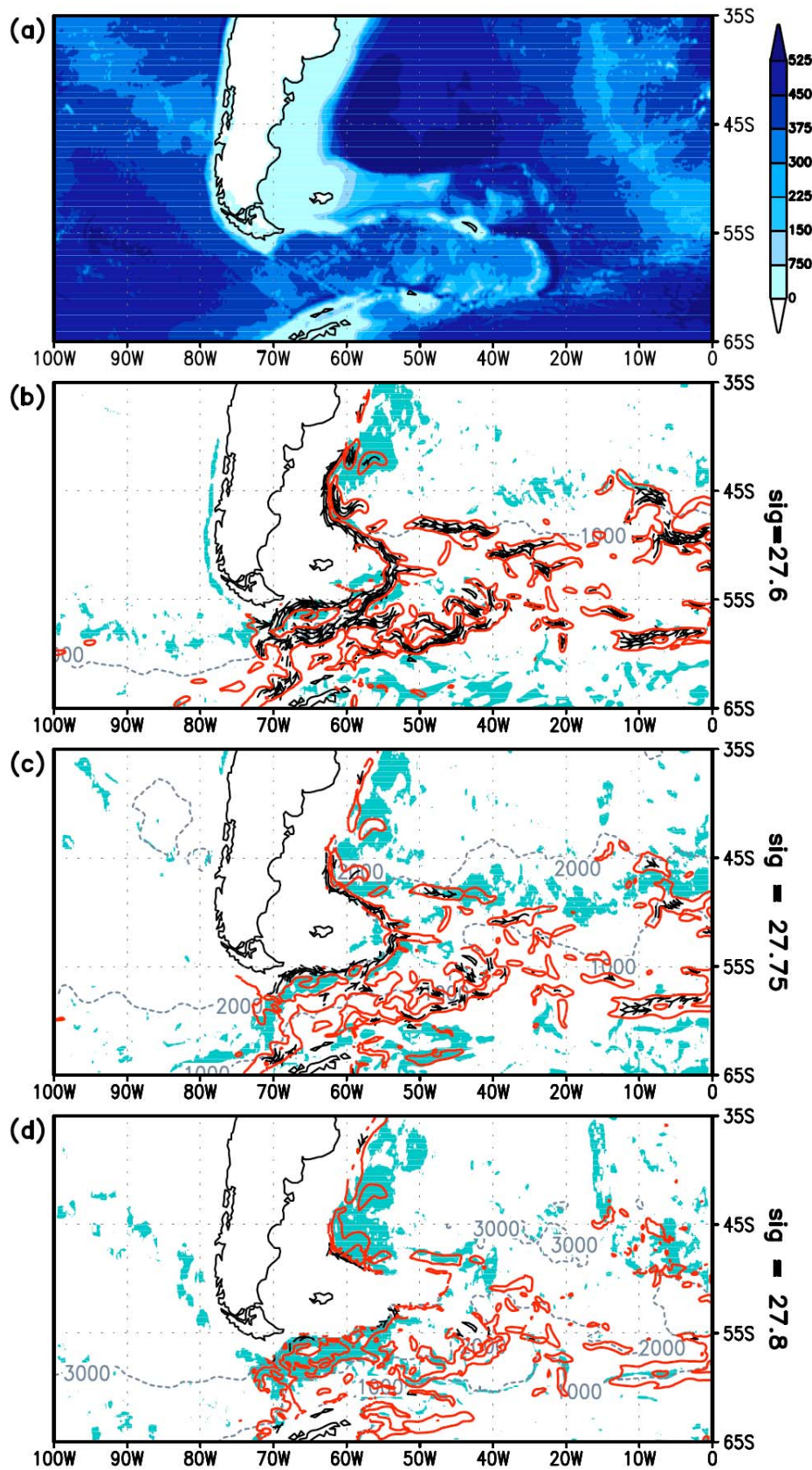


Figure 10. The same as Fig. 7, but for the 100W-0W sector with the isopyncal surfaces in (b) and (c) at 27.6 and 27.75 kg/m<sup>3</sup>.

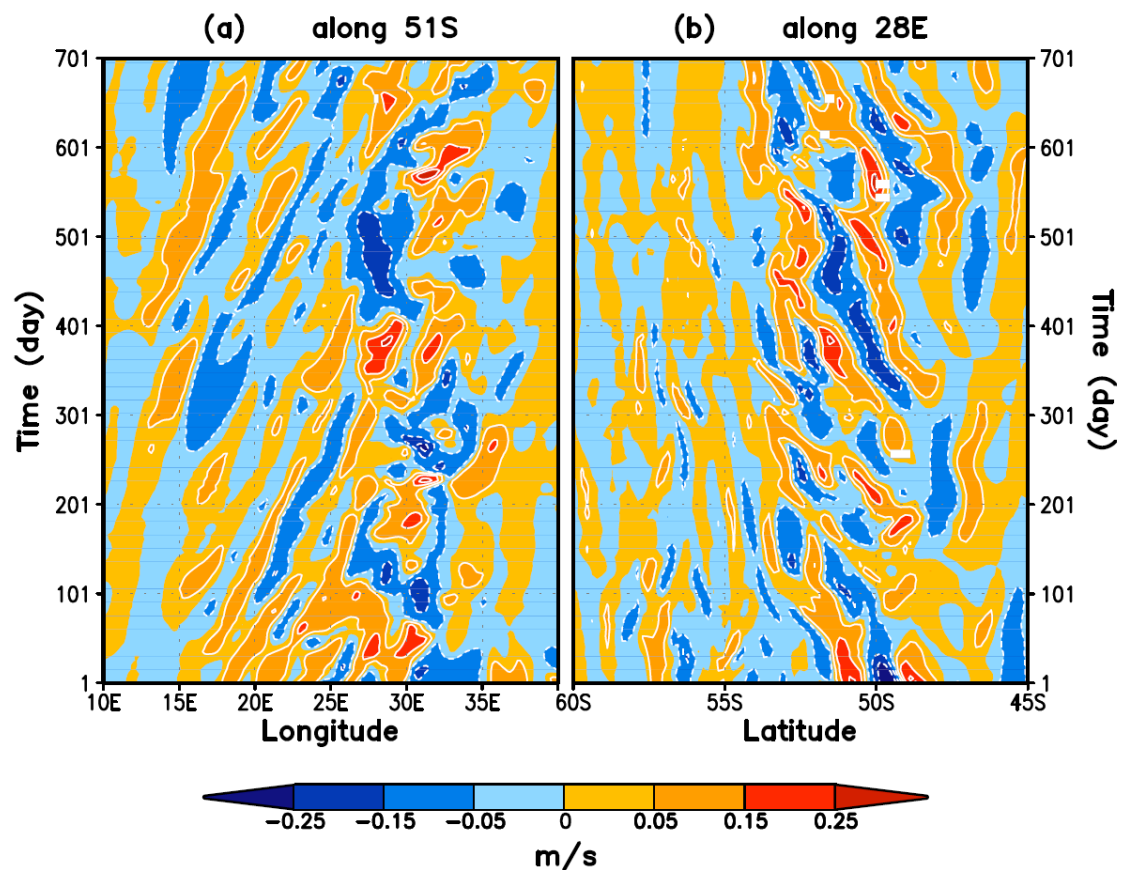


Fig. 11 Hovmöller diagrams of the zonal component of current on the isopycnal surface  $\sigma=27.7 \text{ kg/m}^3$  along 51S and 28E, respectively.